Available online at www.sciencedirect.com

ScienceDirect

Ceramics International 39 (2013) 8615–8622

CERAMICS INTERNATIONAL

www.elsevier.com/locate/ceramint

NO_2 gas sensing properties of Au-functionalized porous ZnO nanosheets enhanced by UV irradiation

Youngho Mun[a], Sunghoon Park[a], Soyeon An[a], Chongmu Lee[a,*], Hyoun Woo Kim[b]

[a]Department of Materials Science and Engineering, Inha University, 253 Yonghyun-dong, Nam-gu, Incheon 402-751, Republic of Korea
[b]Division of Materials Science and Engineering, Hanyang University, Seoul 133-791, Republic of Korea

Received 21 February 2013; received in revised form 10 April 2013; accepted 10 April 2013
Available online 23 April 2013

Abstract

Porous ZnO nanosheets were synthesized by thermal evaporation. The morphology, crystal structure, and sensing properties of the ZnO nanosheets to NO_2 gas at room temperature under UV illumination were examined. Au nanoparticles with diameters of a few tens of nanometers were distributed over the ZnO nanosheets. The responses of the multiple networked nanosheet gas sensors were improved 1.8–3.3 fold by Au functionalization at NO_2 concentrations ranging from 1 to 5 ppm. Furthermore, the Au-functionalized ZnO nanosheet gas sensors showed a considerably enhanced response at room temperature under ultraviolet (UV) illumination. In addition, the mechanisms through which the gas sensing properties of ZnO nanosheets are enhanced by Au functionalization and UV irradiation are discussed.

Keywords: D. ZnO; Au; Functionalization; Gas sensing; Nanosheet

1. Introduction

ZnO is a functional material that is sensitive to toxic and combustible gases [1]. ZnO gas sensors with a range of structures, such as powders [2], thin films [3], heterostructures [4], nanoparticles [5], and one-dimensional nanostructure [6] have been demonstrated. Among these nanostructures, one-dimensional (1D) ZnO nanostructures are particularly useful because of their large length-to-diameter ratio and large surface-to-volume ratio. Studies of the gas sensing properties of ZnO 1D nanostructures focused mainly on CO, H_2S, HCHO, NH_3, H_2, ethanol and humidity [7], whereas there are limited reports on the NO_2 sensing properties of ZnO 1D nanostructures (Table 1) [8–12]. In particular, Zhang et al. compared the sensing properties of brush-like hierarchical ZnO nanostructures to many different types of gases with those of the straight ZnO nanowires [8]. They reported that the brush-like hierarchical ZnO nanostructures exhibited approximately 1.5 fold stronger responses to ethanol and C_6H_6 gases than straight ZnO nanowires, but showed similar responses to the other gases. Regarding the response of ZnO nanostructures to NO_2 gas, the sensitivity of ZnO fiber-mats was reported to be more than 100 toward NO_2 at room temperature [13]. The fiber-mat structure showed an order of magnitude stronger response compared to the cauliflower structure. The difference between the sensing properties of these two structures can be attributed to the differences in their morphologies, because the fiber-mats have more surface available for reaction than the cauliflower structure.

Despite the enhanced gas sensing properties of 1D nanostructures compared to thin films, enhancing their sensing performance and detection limit is still a challenge. A range of techniques such as surface functionalization with novel metals including Pd, Pt and Au [14–17] or doping with novel metals [18–20], MEMS fabrication [21], nanosensing materials [22], application of electrostatic field [23], and ultraviolet (UV) irradiation [24–32] have been developed to reduce the operating temperature and improve the sensitivity and stability of 1D nanostructure-based sensors. Among these techniques, the functionalization of nanowire surfaces with catalyst such as Pd and Pt may be the simplest and most effective technique because the resistance of the sensor changes considerably upon exposure to target gas at room temperature. The optical and electrical properties of the 1D nanostructures coated with catalyst can change upon exposure to gas and can be restored

*Corresponding author. Tel.: +82 32 860 7536; fax: +82 32 862 5546.
E-mail address: cmlee@inha.ac.kr (C. Lee).

0272-8842/$ - see front matter © 2013 Elsevier Ltd and Techna Group S.r.l. All rights reserved.
http://dx.doi.org/10.1016/j.ceramint.2013.04.035

Table 1
Comparison of Au nanoparticles in the Au-functionalized ZnO nanosheets prepared in this study with those in previous studies.

Nanomaterial	Au particle size (nm)	Annealing temperature (°C)	NO_2 concentration (ppm)	Response (%)	Reference
ZnO nanosheets	10–50	700	5	455	Present work
ZnO nanorods	5	–	5	200	[33]
SnO_2 nanowires	20–100	–	10	400	[34]
In_2O_3 thin films	20–30	600	10	140	[35]
CNT	10–40	200	10	110	[36]

upon reexposure to air even at room temperature [14–20]. Such low temperature-processes are desirable for detecting toxic gases safely. UV irradiation is another simple and effective technique. Over the past decade, many studies have shown that UV irradiation improves the sensing performances of semiconducting oxide gas sensors [24–32]. On the other hand, although there have been many reports on the gas sensing properties of one-dimensional nanostructures UV illumination, few studies have examined those of one-dimensional nanostructures functionalized with metal catalyst under UV illumination. This study examined the NO_2 gas sensing properties of multi-networked porous ZnO nanosheets functionalized with Au at room temperature under UV illumination to identify the practical use of ZnO-based gas sensors at room temperature.

2. Experimental

Au-functionalized ZnO nanosheets were synthesized using a three-step process: the synthesis of ZnO nanosheets by the thermal evaporation of Zn powders followed by the sputter-deposition of Au and thermal annealing. First, Au-coated sapphire was used as a substrate for the synthesis of ZnO nanosheet structures. A ~3 nm thick Au thin film was deposited on the (0001) sapphire substrate by direct current (dc) sputtering. A quartz tube was mounted horizontally inside a tube furnace. The 99.99% pure Zn powder was placed on the lower holder at the center of the quartz tube. The Au-coated sapphire substrate was placed on the upper holder approximately 5 mm apart from the Zn powder. The furnace was heated up to 700 °C and maintained at that temperature for 1 h in N_2/3 mol%–O_2 atmosphere with constant flow rates of oxygen (O_2) (3 sccm) and N_2 (100 sccm). The total pressure was set to 1.0 Torr. For the second stage, Au thin film was deposited on the surfaces of some of the as-synthesized ZnO nanosheet samples by direct current (dc) sputtering (substrate temperature: room temperature, power: 20 mA, working pressure: 1.9×10^{-2} Torr, and process time: 100 s). Subsequently, the Au-coated nanosheets were annealed at 700 °C for 1 h in air.

The collected nanosheet samples were characterized by scanning electron microscopy (SEM, Hitachi S-4200), transmission electron microscopy (TEM, Philips CM-200) equipped with an energy-dispersive X-ray spectrometer (EDS) and X-ray diffraction (XRD, Philips X'pert MRD diffractometer). The crystallographic structure was determined by glancing angle XRD using Cu K_α radiation (0.15406 nm) at a scan rate of 2°/min. The sample was arranged geometrically at a 0.5° glancing angle with a rotating detector.

For the sensing measurements, Ni (~10 nm in thickness) and Au (~50 nm) thin films were deposited sequentially by sputtering to form electrodes using an interdigital electrode (IDE) mask. Multiple networked Au-functionalized ZnO nanosheets gas sensors were fabricated by pouring a few drops of nanosheet-suspended ethanol onto oxidized Si substrates equipped with a pair of IDEs and a gap length of 20 μm. The electrical and gas sensing properties of the pristine ZnO nanosheets and Au-functionalized ZnO nanosheets were measured using a home-built computer-controlled characterization system consisting of a test chamber, sensor holder, Keithley sourcemeter-2612, mass flow controllers and a data acquisition system. During the measurements, the nanosheet gas sensors were placed in a sealed quartz tube with an electrical feed through. The test gas was mixed with dry air to achieve the desired concentration, and the flow rate was maintained at 200 sccm using mass flow controllers. The working temperature of the sensors was adjusted by changing the voltage across the heater side. The gas sensing properties of the Au-functionalized ZnO nanosheets were measured at room temperature in a quartz tube placed in a sealed chamber with an electrical feed through. The sensor test was performed by measuring the resistance of the sensor upon controlled concentration of NO_2 gas in the dark and under UV (λ=365 nm) illumination at 1.2 mW/cm^2. The response of the Au-functionalized ZnO nanosheets is defined as R_g/R_a for NO_2, where R_a and R_g are the electrical resistances in the sensors in air and target gas, respectively.

3. Results and discussion

Fig. 1 shows a SEM image of the Au-functionalized ZnO nanosheets synthesized in this study. The synthesis scheme adopted in this study can grow equilateral triangular shaped ZnO nanosheets with a mean base and height of ~0.5 μm and ~1 μm, respectively. The ED spectra obtained by focusing on Au nanoparticle (Fig. 2(a)) and on the ZnO nanosheet (Fig. 2(b)) in Au-functionalized ZnO nanosheet confirmed that the Au-functionalized ZnO nanosheet was composed of Zn, O and Au. The Cu and C in the spectrum were attributed to the TEM grid. The EDS elemental map (Fig. 2(c)) of a typical Au-functionalized ZnO nanosheet showed that Au nanoparticles were distributed sparsely over the surface of the ZnO nanosheet.

The low-magnification TEM image (Fig. 3(a)) shows a typical Au-functionalized ZnO nanosheet. Black and white particles with various sizes were observed on the nanosheet. The white round particles are not real particles but pores, whereas the black round particles are Au nanoparticles. Therefore, the ZnO nanosheet is porous. The diameters of the Au particles ranged from 10 to 50 nm. Table 1 compares

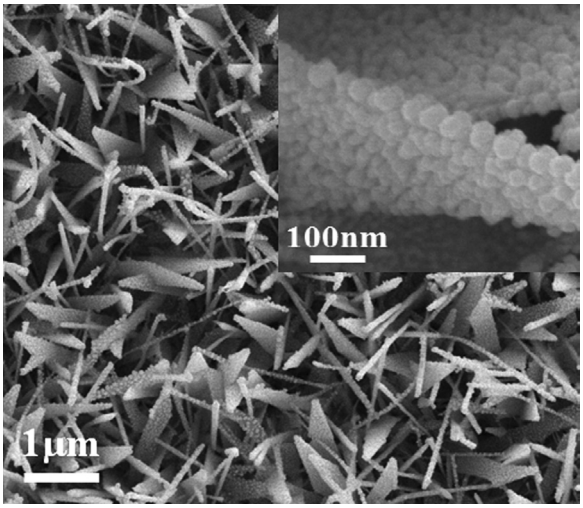

Fig. 1. SEM image of Au-functionalized ZnO nanosheets. Inset, enlarged SEM image of a typical Au-functionalized ZnO nanosheet.

the size of Au nanoparticles and responses of the Au-functionalized ZnO nanosheets sensor fabricated in this study to NO_2 gas with those of other Au-functionalized nanomaterial sensors reported previously [33–36]. The size of Au particles in this study is smaller or comparable to others and the response of the sensor to NO_2 gas measured in this study is higher than those obtained by others. Therefore, we may conclude that the size of Au nanoparticles in the Au-functionalized ZnO nanostructure sensors fabricated in this study is appropriate for efficient gas sensing. Fringe patterns were observed over the entire HRTEM image of the ZnO nanosheet (Fig. 3(b)). The resolved spacing between two neighboring parallel fringes is approximately 0.25 nm, which is in good agreement with the {101} planes of bulk ZnO crystals (JCPDS no. 89-1397, $a=0.3253$ nm, and $c=0.5213$ nm). The corresponding selected area electron diffraction (SAED) pattern recorded perpendicular to the long axis, was indexed to the [010] zone axis of ZnO. The reflection spots in the corresponding selected area electron diffraction (SAED) pattern (Fig. 3(c)) were identified as the (101), (103) and (002) reflections of wurtzite-structured ZnO, indicating that the ZnO nanosheet in the TEM image is a single crystal. Fig. 4 shows the XRD pattern of the as-synthesized Au-functionalized ZnO nanosheets. The main diffraction peaks in the pattern of the as-synthesized nanosheets were indexed to the lattice planes of wurtzite-structured single crystal ZnO, suggestting that the nanomaterial is ZnO.

Fig. 5(a) shows the dynamic responses of the Au-functionalized ZnO nanosheets at room temperature to NO_2 gas under UV illumination at 1.2 mW/cm^2. The resistance increased instantaneously to a maximum resistance, which was maintained at the maximum resistance upon exposure to NO_2 and recovered completely to the initial value upon the removal of NO_2. The sensor responses to NO_2 gas were also stable and reproducible for repeated test cycles. Multiple networked pristine ZnO nanosheets showed responses ranging from ~111 to ~137% at NO_2 concentrations of 1–5 ppm (Table 2). In contrast, the Au-functionalized ZnO nanosheets showed responses ranging from

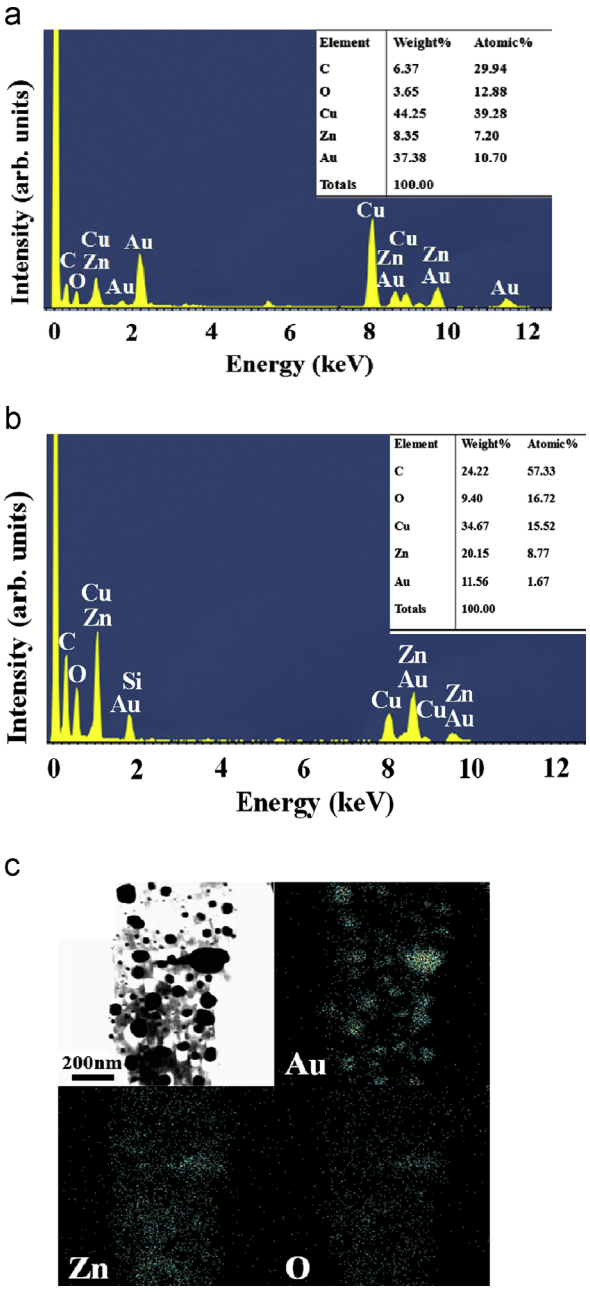

Fig. 2. (a) ED spectrum of a typical Au-functionalized ZnO nanosheet obtained by focusing on an Au nanoparticle. (b) ED spectrum of a typical Au-functionalized ZnO nanosheet obtained by focusing on the ZnO nanosheet. (c) EDS elemental maps of a typical Au-functionalized ZnO nanosheet.

~205 to ~455% over the same concentration range. Therefore, the response of the nanosheets was improved 1.8–3.3 fold at 1–5 ppm NO_2 by the functionalization of ZnO nanosheets with Au.

Fig. 5(d) shows the responses of pristine ZnO nanosheets and Au-functionalized ZnO nanosheets as a function of the NO_2 concentration under UV illumination. The response of an oxide semiconductor is commonly expressed as $R=A[C]^n+B$, where A and B, n, and $[C]$ are constants, exponent and target gas concentration, respectively [37]. Data fitting provided the following equations for the pristine ZnO nanosheets and

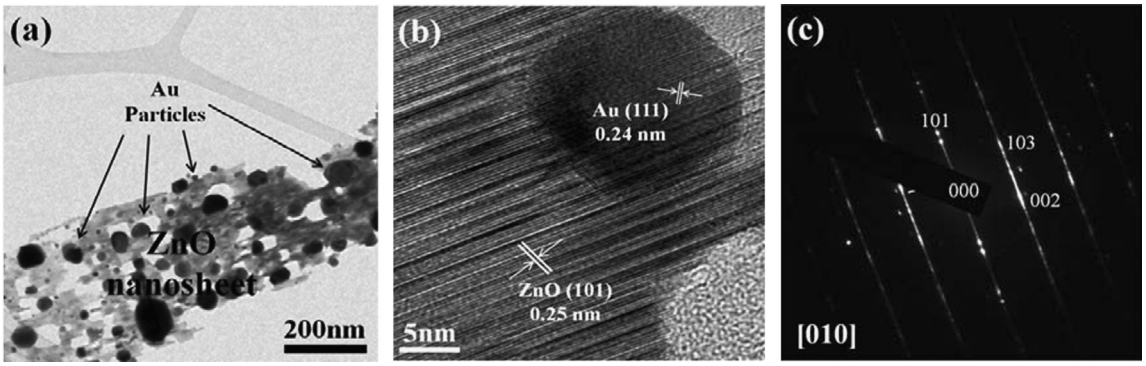

Fig. 3. (a) Low magnification TEM image, (b) high-resolution TEM image, and (c) selected area electron diffraction pattern of Au-functionalized ZnO nanosheets.

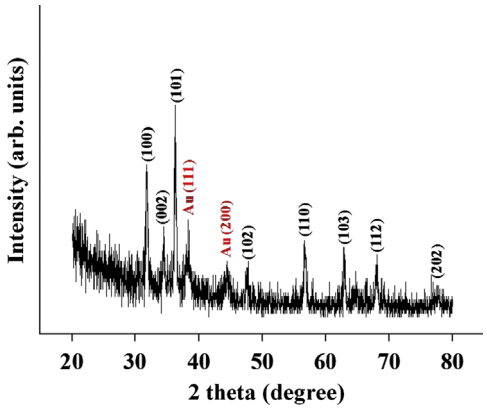

Fig. 4. XRD patterns of Au-functionalized ZnO nanosheets.

Au-functionalized ZnO nanosheets: $R=6.564[C]+102.168$ and $R=62.332[C]+129.636$, respectively. The response of the Au-functionalized ZnO nanosheets tended to increase more rapidly with increasing NO_2 gas concentration than that of the pristine nanosheets, suggesting that the response of the former would be much higher than that of the latter at high NO_2 gas concentrations, such as at a few thousand ppm of NO_2, even though the response of the Au-functionalized ZnO nanosheets was examined only over the NO_2 concentration range 1–5 ppm.

Fig. 6 shows the dynamic responses of the Au-functionalized ZnO nanosheets to 5 ppm NO_2 gas at room temperature under UV illumination with different illumination intensities. The dynamic response of the the Au-functionalized ZnO nanosheets at room temperature without UV light illumination (UV intensity of 0 mW/cm^2) is not shown in Fig. 6 because the change in resistance was negligible and unstable. Table 3 shows that the response of the Au-functionalized ZnO nanosheets to 5 ppm NO_2 increased from ~133 to ~455% with increasing UV illumination intensity from 0.35 to 1.2 mW/cm^2. These high responses at room temperature showed the strong influence of UV light irradiation on the response of the nanosensor to NO_2 gas. This supports previous reports that the UV light irradiation technique enables the realization of room temperature-gas sensors [21–29].

Responses of pristine and Au-functionalized ZnO nanosheet gas sensors to different kinds of gases were compared to examine the selectivity of the gas sensors. The pristine ZnO nanosheet gas sensor showed little difference in response between different gases (Fig. 7), i.e. low selectivity. In contrast, the response of the Au-functionalized ZnO nanosheet sensor to NO_2 gas was far higher than those to CO, H_2S and C_2H_5OH gases. This result shows that selectivity is significantly enhanced by functionalizing ZnO nanosheet with Au. The result also suggests that selectivity is more influenced by Au-functionalization than UV irradiation.

The NO_2 gas sensing mechanism of the Au-functionalized ZnO nanosheets under UV light illumination can be depicted as follows:

When the nanosheets are exposed to air, they interact with oxygen by transferring electrons from the conduction band to the adsorbed oxygen atoms, forming ionic species, such as O^-, O^{2-} and O_2^-, as shown in the following reactions [38,39]:

$$O_2\ (g) \rightarrow O_2\ (ads) \quad (1)$$

$$O_2\ (ads)+e^- \rightarrow O_2^-\ (ads) \quad (2)$$

$$O_2^-\ (ads)+e^- \rightarrow 2O^-\ (ads) \quad (3)$$

$$O^-\ (ads)+e^- \rightarrow O^{2-}\ (ads) \quad (4)$$

A depletion layer is created in the surface region of the nanosheets because electrons in the surface region of the nanosheets are consumed, resulting in a decrease in electrical resistance in the nanosheets. Upon exposure to UV light with photon energy larger than the energy band gap of ZnO, electron–hole pairs will be generated in the ZnO nanosheets. On their way to the surface of the ZnO nanosheets, some of the photo-generated electrons and holes will recombine each other and many of the photo-generated holes react with negatively charged adsorbed oxygen ions on the surface as in the following reactions [30]:

$$h^+(h\nu)+O^{2-}(ads) \rightarrow O_2(g),$$

$$h^+(h\nu)+O^-(ads) \rightarrow 1/2O_2(h\nu),$$

or

$$2h^+(h\nu)+O^{2-}(ads) \rightarrow 1/2O_2(h\nu). \quad (7)$$

As a result of these reactions the width of the surface depletion layer in the nanosheets is reduced. Oxygen species are photodesorbed from the surface. On the other hand, the photo-generated electrons will contribute to the decrease in depletion layer width and resistance.

Upon exposure to NO_2 gas, NO_2 gas adsorbs on the ZnO nanosheets and the remaining photo-generated electrons are

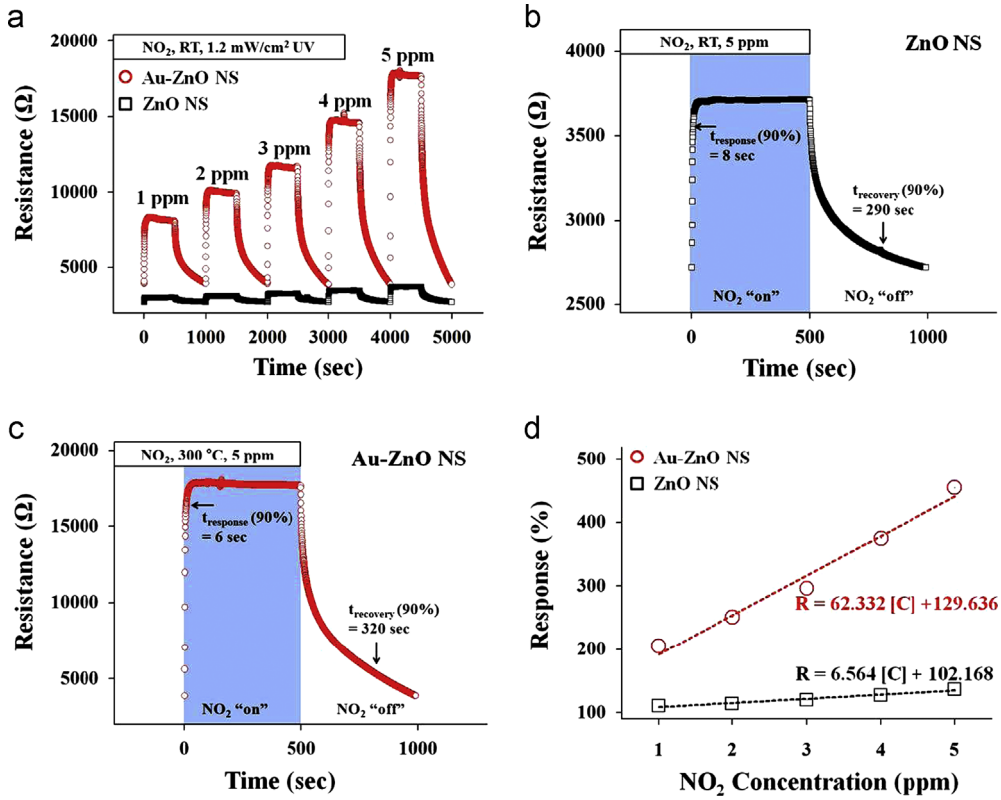

Fig. 5. (a) Dynamic responses of pristine and Au-functionalized ZnO nanosheets to NO_2 gas at 1–5 ppm at room temperature under UV light illumination. (b) Enlarged part of the pristine ZnO nanosheets curve in Fig. 5(a) at 5 ppm NO_2. (c) Enlarged part of the Au-functionalized ZnO nanosheets curve in Fig. 5(a) at 5 ppm NO_2. (d) Responses of pristine and Au-functionalized ZnO nanosheets as a function of the NO_2 gas concentration.

Table 2
Responses measured at different NO_2 concentrations for the Au-functionalized ZnO nanosheet sensor at room temperature under UV illumination at 1.2 mW/cm^2.

NO_2 concentration (ppm).	Response (%)	
	ZnO	Au–ZnO
1	110.78	205.25
2	113.98	251.06
3	120.07	296.90
4	127.76	375.02
5	136.71	454.93

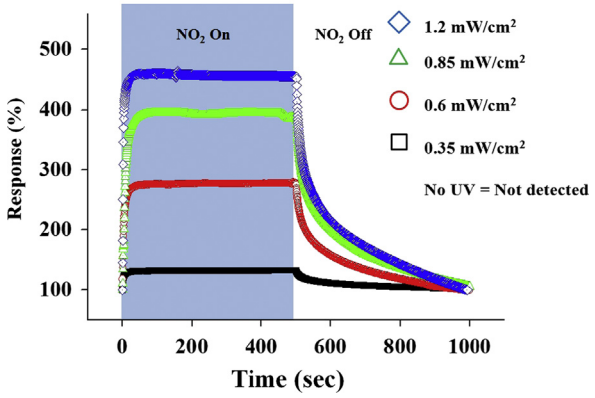

Fig. 6. Dynamic responses of Au-functionalized ZnO nanosheet gas sensors to NO_2 gas at 5 ppm for a range of UV light illumination intensities.

released from the nanosheets, and are attracted to the adsorbed NO_2 molecules because an oxidizing gas, such as NO_2, acts as an electron acceptor, as shown in the following reaction [27]:

$$NO_2\ (g)+e^-\ (h\nu)\rightarrow 2NO\ (h\nu)+O_2^-\ (h\nu) \quad (8)$$

This reaction broadens the surface depletion layer in the ZnO nanosheets, resulting in an increase in the resistance of the nanosheet sensor. Therefore, the depletion layer width and electrical resistance of the sensor increases with increasing NO_2 concentration and UV illumination intensity because the number of electrons participating in the above reaction increases. Undoped ZnO is an n-type semiconductor. Therefore, Au-functionalized ZnO nanosheets have a typical metal-n-type semiconductor contact as shown in the energy band diagram of which is shown in Fig. 8. The depletion layer width (W_{UV}) in the surface region of a ZnO nanosheet under UV illumination is larger than that in the dark (W_{dark}) as shown in Fig. 8.

After the NO_2 gas supply is stopped, the electrons are released to the ZnO nanosheet. This results in an increase in carrier concentration in the ZnO nanosheet and a decrease in the surface depletion layer width. In other words, the electrons are returned to the conduction band, which results in a sharp decrease in electrical resistance in the ZnO nanosheet sensors (Fig. 5(b)).

The significant enhancement in the response of the ZnO nanosheets to NO_2 gas by UV irradiation was attributed to the

increased change in resistance due to the photo-generation of electrons and holes. Briefly, the significant improvement in the response of the ZnO nanosheets to NO_2 gas by UV irradiation was attributed to the increased change in resistance due to an increase in the number of electrons participating in the reactions with NO_2 molecules by photo-generation of electron–hole pairs.

On the other hand, the enhancement of NO_2 gas sensing properties of ZnO nanosheets by Au-functionalization can be explained based on the model proposed for the metal catalyst-enhanced gas sensing of nanomaterials [40]. In the case of Au-functionalized ZnO nanosheets, the NO_2 gas was spilt over the ZnO nanosheet surface by Au nanoparticles and the chemisorption and dissociation of NO_2 gas was enhanced on the Au nanoparticle surface due to the high catalytic or conductive nature of Au. Consequently, the number of electrons attracted to the gas increases. In addition, localized surface plasmon forms in an Au nanoparticle at the surfaces of Au-functionalized ZnO nanosheets as shown in Fig. 8. Therefore, electrons transfer from the defect states in ZnO nanosheets to the Au nanoparticles in Au-functionalized ZnO nanosheets. This electron transfer from the defect states to the Au nanoparticles not only results in an increase in resonant electron density, but also creates energetic electrons in higher energy state [41,42]. These resonant electrons are so active that they can escape from the surface of Au nanoparticles to the conduction band of the ZnO nanosheets. Therefore, the electron density in the conduction band of ZnO is increased significantly by Au-functionalization. Briefly, the increase in the number of electrons by the transfer of electrons from the localized surface plasmon in Au nanoparticles to the conduction band of ZnO as well as combination of the spillover effect and the enhancement of chemisorption and dissociation of gas results in the enhanced electrical response of the Au-functionalized ZnO nanosheet sensor to NO_2 gas.

Table 3
Responses of the Au-functionalized ZnO nanosheet sensor to 5 ppm NO_2 measured at room temperature for different UV illumination intensities.

UV power (mW/cm^2)	Response (%)
0.35	132.86
0.6	280.11
0.85	388.31
1.2	454.93

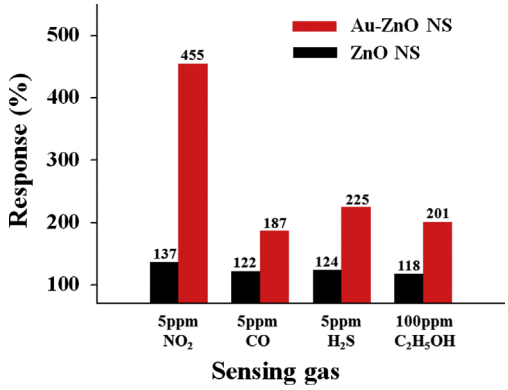

Fig. 7. Comparison of responses of pristine and Au-functionalized ZnO nanosheets gas sensors to different kinds of gases.

4. Conclusions

Au-functionalized porous ZnO nanosheets were synthesized using a three-step process: synthesis of ZnO nanosheets by the thermal evaporation of Zn powders followed by Au sputter-deposition and thermal annealing. The multiple networked pristine ZnO nanosheets showed responses ranging from ~111 to ~137% at NO_2 concentrations ranging from 1 to 5 ppm

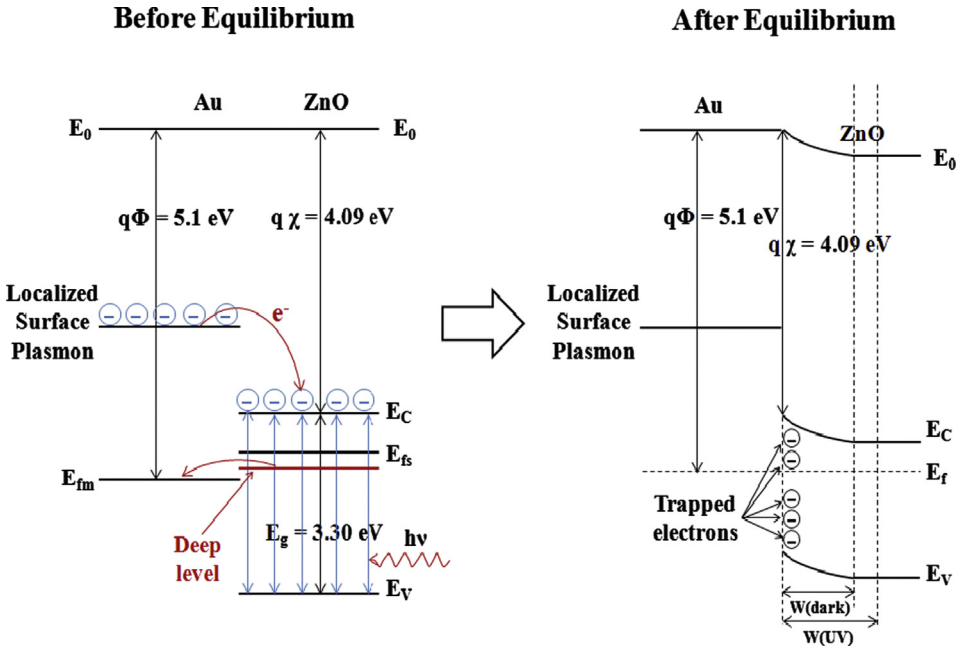

Fig. 8. Energy band diagrams of the Au–ZnO system before and after equilibrium.

(Table 1). In contrast, the Au-functionalized ZnO nanosheets showed responses ranging from ~205 to ~455% over the same concentration range. Therefore, the response of the nanosheets was increased 1.8–3.3 fold at 1–5 ppm NO_2 by the functionalization of ZnO nanosheets with Au. The response of the Au-functionalized ZnO nanosheets increased from ~133 to ~455% with increasing UV illumination intensity from 0.35 to 1.2 mW/cm^2. The significant enhancement in the response of the ZnO nanosheets to NO_2 gas by UV irradiation was attributed to the increased change in resistance due to the photo-generation of electrons and holes.

Acknowledgment

This work was supported by the Key Research Institute Program' through the National Research Foundation of Korea (NRF) funded by the Ministry of Education, Science and Technology (2011–0018394).

References

[1] J. Xu, Q. Pan, Y. Shun, Z. Tian, Grain size control and gas sensing properties of ZnO gas sensor, Sensors and Actuators B 66 (2000) 277–279.
[2] M.S. Wagh, G.H. Jain, D.R. Patil, S.A. Patil, L.A. Patil, Modified zinc oxide thick film resistors as NH_3 gas sensor, Sensors and Actuators B 115 (2006) 128–133.
[3] J. Wöllenstein, J.A. Plaza, C. Can´e, Y. Min, H. Böttner, H.L. Tuller, A novel single chip thin film metal oxide array, Sensors and Actuators B 93 (2003) 350–355.
[4] S. Mridha, D. Basak, Investigation of a p-CuO/n-ZnO thin film heterojunction for H_2 gas-sensor applications, Semiconductor Science and Technology 21 (2006) 928–932.
[5] G.G. Huang, C.T. Wang, H.T. Tang, Y.S. Huang, J. Yang, ZnO nanoparticle-modified infrared internal reflection elements for selective detection of volatile organic compounds, Analytical Chemistry 78 (2006) 2397–2404.
[6] Y. Sun, N. George Ndifor-Angwafor, D. Jason Riley, M.N.R. Ashfold, Synthesis and photoluminescence of ultrathin ZnO nanowire/nanotube arrays formed by hydrothermal growth, Chemical Physics Letters 431 (2006) 352–357.
[7] M.M. Arafat, B. Dinan, S.A. Akbar, A.S.M.A. Haseeb, Gas sensors based on one dimensional nanostructured metal-oxides: a review, Sensors 12 (2012) 7207–7258.
[8] Y. Zhang, J. Xu, X. Jiang, H. Li, Q. Pan, P. Xu, Brush-like hierarchical ZnO nanostructures: synthesis, photoluminescence and gas sensor properties, Journal of Physical Chemistry C 113 (2009) 3430–3435.
[9] J. Moon, J.A. Park, S.J. Lee, T. Zyung, Semiconducting ZnO nanofibers as gas sensors and gas response improvement by SnO_2 coating, ETRI Journal 31 (2009) 636–641.
[10] E. Oh, H.Y. Choi, S.H. Jung, S. Cho, J.C. Kim, K.H. Lee, S.W. Kang, J. Kim, J.Y. Yun, S.H. Jeong, High-performance NO_2 gas sensor based on ZnO nanorod grown by ultrasonic irradiation, Sensors and Actuators B 141 (2009) 239–243.
[11] P.S. Cho, K.W. Kim, J.H. Lee, NO_2 sensing characteristics of ZnO nanorods prepared by hydrothermal method, Journal of Electroceramics 17 (2006) 975–978.
[12] F.T. Liu, S.F. Gao, S.K. Pei, S.C. Tseng, C.H.J. Liu, ZnO nanorod gas sensor for NO_2 detection, Journal of the Taiwan Institute of Chemical Engineers 40 (2009) 528–532.
[13] C. Baratto, G. Sberveglieri, A. Onischuk, B. Caruso, S. di Stasio, Low temperature selective NO_2 sensors by nanostructured fibres of ZnO, Sensors and Actuators B 100 (2004) 261–265.
[14] X. Liu, J. Zhang, X. Guo, S. Wu, S. Wang, Amino acid-assisted one-pot assembly of Au, Pt nanoparticles onto one-dimensional ZnO microrods, Nanoscale 2 (2010) 1178–1184.
[15] X. Liu, J. Zhang, L. Wang, T. Yang, X. Guo, S. Wu, S. Wang, 3D hierarchically porous ZnO structures and their functionalization by Au nanoparticles for gas sensors, Journal of Materials Chemistry 21 (2011) 349–356.
[16] X. Liu, J. Zhang, T. Yang, X. Guo, S. Wu, S. Wang, Synthesis of Pt nanoparticles functionalized WO_3 nanorods and their gas sensing properties, Sensors and Actuators B 156 (2011) 918–923.
[17] J. Zhang, X. Liu, M. Xu, X. Guo, S. Wu, S. Zhang, S. Wang, Pt clusters supported on WO_3 for ethanol detection, Sensors and Actuators B 147 (2010) 185–190.
[18] G. Gundiah, A. Govindarj, C.N.R. Rao, Nanowires, nanobelts and related nanostructures of Ga_2O_3, Chemical Physics Letters 351 (2002) 189–194.
[19] Y.H. Gao, Y. Bando, T. Sato, Synthesis, Raman scattering and defects of β-Ga_2O_3 nanorods, Applied Physics Letters 81 (2002) 2267–2269.
[20] H. Kim, C. Jin, S. Park, S. Kim, C. Lee, H_2S gas sensing properties of bare and Pd-functionalized CuO nanorods, Sensors and Actuators B 161 (2012) 594–599.
[21] S.P. Arnold, S.M. Prokes, K. Perkins, M.E. Zaghloul, Design and performance of a simple, room-temperature Ga_2O_3 nanowire gas sensor, Applied Physics Letters 95 (2009) 103102.
[22] Y.J. Choi, I.S. Hwang, J.G. Park, K.J. Choi, J.H. Park, J.H. Lee, Novel fabrication of an SnO_2 nanowire gas sensor with high sensitivity, Nanotechnology 19 (2008) 095508.
[23] Y. Zhang, A. Kolmakov, Y. Lilach, M. Moskovits, Electronic control of chemistry and catalysis at the surface of an individual tin oxide nanowire, Journal of Physical Chemistry B 109 (2005) 1923–1929.
[24] E. Comini, A. Cristalli, G. Faglia, G. Sberveglieri, Light enhanced gas sensing properties of indium oxide and tin dioxide sensors, Sensors and Actuators B 65 (2000) 260–263.
[25] E. Comini, G. Faglia, G. Sberveglieri, UV light activation of tin oxide thin films for NO_2 sensing at low temperatures, Sensors and Actuators B 78 (2001) 73–77.
[26] J.D. Prades, R.J. Diaz, F.H. Ramirez, S. Barth, A. Cirera, A.R. Rodriguez, S. Mathur, J.R. Morante, Equivalence between thermal and room temperature UV light modulated responses of gas sensors based on individual SnO_2 nanowires, Sensors and Actuators B 140 (2009) 337–341.
[27] S.W. Fan, A.K. Srivastava, V.P. Dravid, UV-activated room-temperature gas sensing mechanism of polycrystalline ZnO, Applied Physics Letters 95 (2009) 142106.
[28] S.W. Fan, A.K. Srivastava, V.P. Dravid, Nanopatterned polycrystalline ZnO for room temperature gas sensing, Sensors and Actuators B 144 (2010) 159–163.
[29] J. Gong, Y.H. Li, X.S. Chai, Z.S. Hu, Y.L. Deng, UV-light-activated ZnO fibers for organic gas sensing at room temperature, Journal of Physical Chemistry C 114 (2010) 1293–1298.
[30] C.L. Cao, C.G. Hu, X. Wang, S.X. Wang, Y.S. Tian, H.L. Zhang, UV sensor based on TiO_2 nanorod arrays on FTO thin film, Sensors and Actuators B 156 (2011) 114–119.
[31] O. Lupana, L. Chowa, G. Chaid, A single ZnO tetrapod-based sensor, Sensors and Actuators B 141 (2009) 511–517.
[32] G. Lu, J. Xu, J. Sun, Y. Yu, Y. Zhang, F. Liu, UV-enhanced room temperature NO_2 sensor using ZnO nanorods modified with SnO_2 nanoparticles, Sensors and Actuators B 162 (2012) 82–88.
[33] P. Rai, Y.S. Kim, H.M. Song, M.K. Song, Y.T. Yu, The role of gold catalyst on the sensing behavior of ZnO nanorods for CO and NO_2 gases, Sensors and Actuators B 165 (2012) 133–142.
[34] S.W. Choi, S.H. Jung, S.S. Kim, Significant enhancement of the NO_2 sensing capability in networked SnO_2 nanowires by Au nanoparticles synthesized via γ-ray radiolysis, Journal of Hazardous Materials 193 (2011) 243–248.
[35] H. Steffes, C. Imawan, F. Solzbacher, E. Obermeier, Enhancement of NO_2 sensing properties of In_2O_3-based thin films using an Au or Ti surface modification, Sensors and Actuators B 78 (2001) 106–112.
[36] M. Penza, R. Rossi, M. Alvisi, G. Cassano, E. Serra, Functional characterization of carbon nanotube networked films functionalized with tuned loading of Au nanoclusters for gas sensing applications, Sensors and Actuators B 140 (2009) 176–184.
[37] D.E. Williams, Solid State Gas Sensors, Hilger, Bristol, 1987.

[38] N. Barsan, U. Weimar, Conduction model of metal oxide gas sensors, Journal of Electroceramics 7 (2001) 143–167.
[39] N. Yamazoe, Oxide semiconductor gas sensors, Catalysis Surveys from Asia 7 (2003) 63–75.
[40] A. Kolmakov, D. Klenov, Y. Lilach, S. Stemmer, M. Moskovits, Enhanced gas sensing by individual SnO_2 nanowires and nanobelts functionalized with Pd catalyst particles, Nano Letters 5 (2005) 667–673.
[41] C. Sonnichsen, T. Franzl, T. Wilk, G. von Plessen, J. Feldmann, Drastic reduction of plasmon damping in gold nanorods, Physical Review Letters 88 (2002) 077402.
[42] Y. Zhang, X. Li, X. Ren, Effects of localized surface plasmons on the photoluminescence properties of Au-coated ZnO films, Optics Express 17 (2009) 8735–8740.